Thermodynamic and diamagnetic properties of weakly doped antiferromagnets

Darko Veberič*

Jožef Stefan Institute, SI-1000 Ljubljana, Slovenia

Peter Prelovšek[†]

Jožef Stefan Institute, SI-1000 Ljubljana, Slovenia
and Faculty of Mathematics and Physics, University of Ljubljana, SI-1000 Ljubljana, Slovenia

Hans Gerd Evertz[‡]

Institute for Theoretical Physics, Technical University Graz, 8010 Graz, Austria

(Received 14 February 2000)

The finite-temperature properties of weakly doped antiferromagnets as modeled by the two-dimensional *t-J* model and relevant to underdoped cuprates are investigated by numerical studies of small model systems at low doping. Two numerical methods are used: the world line quantum Monte Carlo method with a loop cluster algorithm and the finite-temperature Lanczos method, yielding consistent results. The thermodynamic quantities—specific heat, entropy, and spin susceptibility—reveal a sizable perturbation induced by holes introduced into a magnetic insulator, as well as a pronounced temperature dependence. The diamagnetic susceptibility introduced by a coupling of the magnetic field to the orbital current reveals an anomalous temperature dependence, changing character from diamagnetic to paramagnetic at intermediate temperatures.

I. INTRODUCTION

The anomalous normal-state properties of superconducting cuprates[1] have stimulated intense theoretical investigations of models of strongly correlated electrons describing the interplay between antiferromagnetic (AFM) ordering of reference (undoped) insulating substances and the itinerant character of charge carriers introduced by doping. For the understanding of superconductivity the most challenging regime is that of intermediate (optimum) doping. However, even the apparently simplest region of weak doping is not fully understood theoretically.

Recently, attention in experimental and theoretical investigations of cuprates has been given to the characterization and understanding of different doping regimes.[2] In a simple picture, weak doping should correspond to the regime where properties vary linearly with concentration of holes: i.e., one can deal with a semiconductorlike model where charge carriers (holes) are independent and well-defined quasiparticles. This requires a nonsingular variation of thermodynamic quantities with doping. However, this scenario has been questioned near the metal-insulator transition based also on numerical solutions for some model systems,[1] e.g., the Hubbard model. Alternative possibilities include phase separation,[3] quantum critical behavior,[4] or other instabilities at low doping. Still, singular behavior in a planar [two-dimensional (2D)] system is expected only at $T=0$, while $T>0$ should lead to a regular variation with doping.

Among the least understood properties of charge carriers in cuprates and correlated systems in general are those related to the coupling of their orbital motion to an external magnetic field. Evidently anomalous and not understood is the Hall constant in cuprates which reveals unusual temperature and doping dependence.[5] Another quantity is the diamagnetic (orbital) susceptibility χ_d, which for noninteracting electrons corresponds to Landau diamagnetism[6] and seems to be connected to the Hall response.[7] An anomalous paramagneticlike variation with magnetic field has been noticed within the ground state of the *t-J* model[8] at low doping. Recent $T>0$ studies of a single hole within the *t-J* model[9] confirm the existence of a paramagnetic regime at intermediate *T*, though the systems studied were quite small. Conclusive experimental results on diamagnetic susceptibility are lacking,[10] since the orbital part appears quite hidden by other contributions, although it could be distinguished via the anisotropy.

The aim of this paper is to study the thermodynamic properties and orbital response of correlated electrons at finite temperature in the low-doping regime. Most numerical studies of the *t-J* model have so far focused on the ground-state properties,[11] employing exact diagonalization of small systems, projector Monte Carlo techniques, and density matrix renormalization group[12] (DMRG). Recently, the finite-temperature Lanczos method (FTLM) has been introduced, which allows insight into the statics and dynamics at $T>0$. In previous applications certain thermodynamic quantities have also been investigated as a function of doping. In this paper we focus on the low-doping regime, where the method can be compared with the alternative approach, an adaptation of the world line quantum Monte Carlo (QMC) cluster method[13] which allows for the study of much larger systems at least for temperatures $T>T_-$ below which the minus-sign problem sets in. Large systems are particularly important for the study of the diamagnetic response which appears to be quite sensitive to finite-size effects. In both cases, ways of dealing with the magnetic field are introduced. Related QMC methods have been used to study the nonmagnetic properties of the *t-J* model, in an exploratory calculation for doped chains and for ladders with 1 and 2 holes,[15] in two dimen-

sions at $J \to 0$ with 1 or 2 holes[16] and for chains at finite J in a background of no holes.[14]

In the following, the planar t-J model as a representative model for strongly correlated electrons and electronic properties of cuprates is studied,

$$H = -t \sum_{\langle ij \rangle \sigma} (\tilde{c}_{j\sigma}^\dagger \tilde{c}_{i\sigma} + \text{H.c.}) + J \sum_{\langle ij \rangle} \left(\mathbf{S}_i \cdot \mathbf{S}_j - \frac{1}{4} n_i n_j \right), \quad (1)$$

where $\tilde{c}_{i\sigma}^\dagger$ and $\tilde{c}_{i\sigma}$ are fermionic operators, projecting out sites with double occupancy. To approach the regime of strong correlations close to the real situation in cuprates, $J/t = 0.4$ is used in most numerical calculations. We also use $k_B = \hbar = 1$.

The paper is organized as follows. Section II of the paper is devoted to a brief introduction of both numerical techniques employed, QMC and the FTLM. In Sec. III results for several thermodynamic properties in the low-doping regime are presented and discussed. Section IV is devoted to a discussion of the orbital susceptibility of the system.

II. NUMERICAL METHODS

Results are obtained independently by the world line QMC method and the FTLM. Wherever possible, results of both methods for doped systems are compared and presented relative to the undoped Heisenberg AFM. For large enough systems, we expect to reach a typical behavior in the low-doping regime.

A. World line quantum Monte Carlo method

The loop cluster algorithm (LCA) for the world line QMC has been introduced by one of the present authors[13] and recently adapted also to the t-J model.[15,16]

We briefly describe the world line representation of the QMC. The Hamiltonian, Eq. (1), on a 2D square lattice can be split within the standard Trotter-Suzuki decomposition[17,18] into four parts $H = H_1 + H_2 + H_3 + H_4$ consisting of mutually commuting terms. This is equivalent to the well-known checkerboard decomposition of Hamiltonians in 1D. The partition function is

$$Z = \text{Tr } e^{-\beta H} = \lim_{M \to \infty} \text{Tr}[e^{-\tilde{\beta}(H_1 + H_2 + H_3 + H_4)}]^M$$

$$= \text{Tr}[e^{-\tilde{\beta} H_1} e^{-\tilde{\beta} H_2} e^{-\tilde{\beta} H_3} e^{-\tilde{\beta} H_4}]^M + O(\tilde{\beta}^2)$$

$$\approx \sum_{\phi_1 \cdots \phi_{4M}} \langle \phi_{4M} | e^{-\tilde{\beta} H_1} | \phi_1 \rangle$$

$$\times \langle \phi_1 | e^{-\tilde{\beta} H_2} | \phi_2 \rangle \cdots \langle \phi_{4M-1} | e^{-\tilde{\beta} H_4} | \phi_{4M} \rangle, \quad (2)$$

where $\tilde{\beta} = \beta/M$ and $\beta = 1/T$. The summation is taken over the complete orthonormal set of states $|\phi_i\rangle$. Within each imaginary time step $\tilde{\beta}$, the time evolution operator is applied. Since the Hamiltonian is total spin conserving, we can track time evolution of a particular spin along its so called *world line* (WL). Because of the cyclic property of the trace, the WLs are periodic in the imaginary time interval $[0, \beta]$. The time evolution operator acts only on 2×2 plaquettes,

and the weight of the configuration $W(\mathcal{C})$ factorizes into a product of plaquette weights. The partition function

$$Z = \sum_{\mathcal{C}} W(\mathcal{C}) = \sum_{\mathcal{C}} \prod_{p \in \mathcal{C}} W(p) \quad (3)$$

is formally that of a $(2+1)$-dimensional classical system. The thermal average of an observable $\mathcal{O}$ can be obtained by

$$(\mathcal{O}) = \frac{1}{Z} \sum_{\mathcal{C}} W(\mathcal{C}) \mathcal{O}(\mathcal{C}). \quad (4)$$

Such thermal expectation values are calculated by means of Monte Carlo (MC) importance sampling, where a sequence of configurations $\mathcal{C}_i$ (Markov chain) is constructed, which obeys detailed balance and reproduces the correct Boltzmann distribution $W(\mathcal{C})/Z$. Thermal expectation values now become simple averages

$$\langle \mathcal{O} \rangle = \lim_{K \to \infty} \frac{1}{K} \sum_i^K \mathcal{O}(\mathcal{C}_i). \quad (5)$$

In practice, Monte Carlo runs are finite, $K < \infty$, leading to statistical errors which can be calculated from the standard deviation of partial data sets.[13]

In standard local algorithms an update from one configuration $\mathcal{C}$ to another $\mathcal{C}'$ in the Markov chain represents a small local change of the WLs. Therefore, consecutive configurations are highly correlated, which drastically increases the necessary number of Monte Carlo steps. Such difficulties are overcome in the LCA,[13] which introduces global (nonlocal) stochastic updates that effectively reduce the correlations. In the LCA formulation also the continuous time limit $\tilde{\beta} \to 0$ can be taken,[19] avoiding the second-order systematic error of Eq. (2). For certain observables improved estimators can be easily constructed, allowing a potential reduction of statistical errors. For more details we refer to the introductory paper in Ref. 13.

The LCA has recently been adapted to the t-J model. The update procedure is split into three substeps, allowing the application of the standard LCA for the $S = 1/2$ antiferromagnetic Heisenberg model or for free fermions in all three cases. Within each substep, only updates between two of the possible three states ($\uparrow$, $\downarrow$, and hole $\circ$) are performed. For the weights of particular plaquettes and other technical details we refer to Ref. 15.

In case of negative weights $W(\mathcal{C}) < 0$, their magnitude $|W(\mathcal{C})|$ is taken for construction of the MC procedure, since the negative $W(\mathcal{C})$ cannot be taken as a probability. Equation (4) becomes
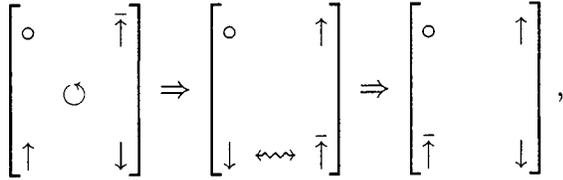
$$\langle \mathcal{O} \rangle = \frac{\langle \text{sign} \times \mathcal{O} \rangle_{|W|}}{\langle \text{sign} \rangle_{|W|}}, \quad (6)$$

where $\langle \cdots \rangle_{|W|}$ denotes the expectation value with respect to the absolute value of the weight. In systems with such a "sign problem," the average sign $\langle \text{sign} \rangle_{|W|}$ often becomes exponentially small with increasing system size and decreasing temperature T, leading to a blowup of statistical errors.[18]

Let us briefly comment on the origin of negative signs in the WL formulation of the t-J model. In the system with no doped holes, the only source of negative weights are

plaquettes, where two opposite spins exchange their positions representing a spin flip. Because of the periodicity of WLs in time direction and the absence of holes, spin flips always occur in even numbers, producing no net negative sign. In the pure Heisenberg model, this sign can also be transformed away by rotation of spins on one sublattice, resulting in all-positive plaquette weights.[13]

For one hole doped into the AFM, one would naively not expect a sign problem: e.g., in this case there is no sign in the exact diagonalization approach. Examining the particle WLs surrounding the hole WL, one finds, however, that an exchange of two fermions can occur when $t \neq 0$ and $J \neq 0$, producing an odd number of spin flips, i.e., a negative sign, as can be seen schematically in a small 2×2 system,

$$
\begin{bmatrix} \circ & \bar{\uparrow} \\ \circlearrowleft & \\ \uparrow & \downarrow \end{bmatrix} \Rightarrow \begin{bmatrix} \circ & \uparrow \\ \downarrow & \leftrightsquigarrow \bar{\uparrow} \end{bmatrix} \Rightarrow \begin{bmatrix} \circ & \uparrow \\ \bar{\uparrow} & \downarrow \end{bmatrix},
$$

where a loop motion of the hole $\circlearrowleft$ around the system and a consecutive spin flip $\leftrightsquigarrow$ reproduce the original configuration with two fermions $\uparrow$ and $\bar{\uparrow}$ interchanged. Measuring the sign here reduces to spin flip counting.

For higher concentration of holes, a more general expression for the sign of the configuration can be obtained. It links the fermion WL (perm$_f$) and hole WL permutation (perm$_h$),

$$
\text{sgn}(\mathcal{C}) = (-1)^{\text{perm}_f} = (-1)^{\text{perm}_h} \text{sgn}[W(\mathcal{C})], \tag{7}
$$

so that for low doping it is preferable to measure perm$_h$ rather than perm$_f$. The sign problem also complicates the use of the improved estimators since for every observable a separate algorithm must be devised.

To follow the emergence of the sign problem as well as the development of diamagnetic properties, it is convenient to generalize the isotropic spin interaction term of the model Eq. (1) to an anisotropic one with general anisotropy parameter γ:

$$
H_J = J \sum_{\langle ij \rangle} \left[\frac{\gamma}{2} (S_i^+ S_j^- + S_j^+ S_i^-) + S_i^z S_j^z \right]. \tag{8}
$$

This modifies the pure spin substep $(\uparrow, \downarrow)$ of the t-J LCA so that otherwise independent loops are ''frozen'' together[13] into clusters and updated stohasticaly.

The results for $\langle \text{sign} \rangle$ as a function of inverse temperature $\beta t = 1/k_B T$ are presented in Fig. 1. Note that for a single hole in the system, $N_h = 1$, the relevant temperature scale in the anisotropic case is $T_- \sim \gamma J$: i.e., there is no sign problem for $\gamma = 0$. At $T \lesssim T_-$ the sign starts to deteriorate rapidly, as can be seen in Fig. 1, preventing the investigation of low-temperature properties. As expected $\langle \text{sign} \rangle$ decreases by adding additional holes $N_h > 1$. For this reason, within the doped t-J model only chains and coupled chains[15] have been investigated by the LCA so far, and in two dimensions the limit $J \rightarrow 0$ with $N_h = 1, 2$.[16] Recently, though, a way around the sign problem has been proposed by calculating fermion propagators for a background of no holes.[14]
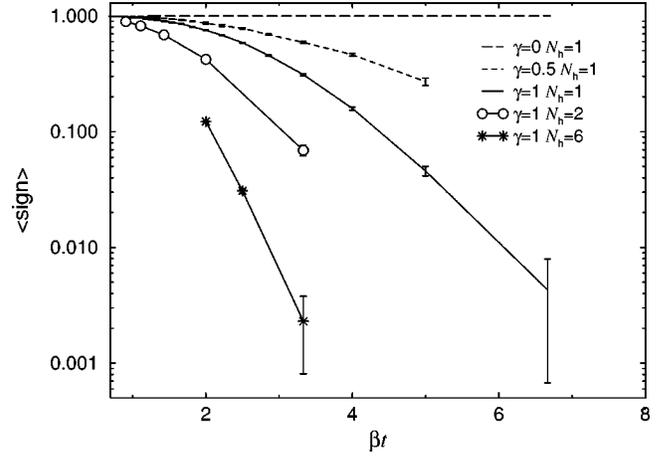

FIG. 1. Average sign in QMC for different values of the anisotropy γ and number of holes N_h for a 6×6 system with $J = 0.4t$.

For a fixed number of holes, the average sign will converge as the system size increases. This convergence could be taken as a another criterion that the limit of a dilute system has been reached.

B. Finite-temperature Lanczos method

In the analysis of the t-J model, the exact diagonalization of small systems using the Lanczos algorithm has been extensively employed,[11] predominantly in the investigation of the static and dynamic properties of the ground state. More recently, a FTLM combining the Lanczos procedure and random sampling was introduced,[20,21] allowing the calculation of $T > 0$ static and dynamic properties of correlated systems. The application is particularly simple for an arbitrary function of conserved quantities, e.g., $f(H, S_z)$,

$$
Z \approx \frac{N_{\text{st}}}{K} \sum_{n=1}^{K} \sum_{i=0}^{M-1} e^{-\beta E_i^n} |\langle n | \psi_i^n \rangle|^2, \tag{9}
$$

$$
\langle f \rangle \approx \frac{N_{\text{st}}}{KZ} \sum_{n=1}^{K} \sum_{i=0}^{M-1} f(E_i^n, S_z^n) e^{-\beta E_i^n} |\langle n | \psi_i^n \rangle|^2, \tag{10}
$$

where $|\psi_i^n \rangle$ and E_i^n are (approximate) eigenfunctions and energies, respectively, obtained by diagonalization within the reduced orthonormal set, generated from the initial functions $|n\rangle$ in M Lanczos steps. N_{st} is the dimension of the complete basis. K initial function $|n\rangle$ are chosen at random, but with good quantum number S_z. Usually, it is enough to choose $M, K \ll N_{\text{st}}$. For a more detailed discussion of the method and results, we refer to Ref. 21.

It is expected that $T > 0$ reduces the finite-size effects of the measured quantities. It is, however, important to realize that for a particular system, finite-size effects start to be pronounced at $T < T_{\text{fs}}$ where, e.g., some characteristic length scale becomes larger than the system size. In our case of low doping, $N \leq 20$ and $J = 0.4t$, we find $T_{\text{fs}} \sim 0.4J$. All our results are presented for $T > T_{\text{fs}}$ where $Z(T_{\text{fs}}) \sim Z^*$. In the present study, $Z^* = 30$, so that at least 30 states are sampled

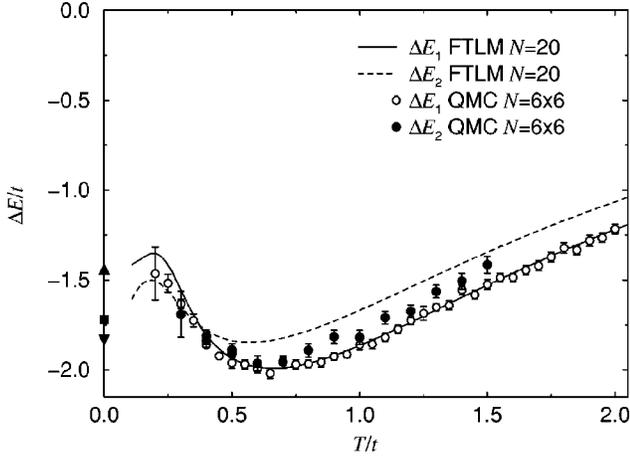FIG. 2. Internal energy per hole ΔE vs T as calculated within the FTLM and the QMC method for $J=0.4t$. ■ represents the one-hole ground state result for $N=4\times4$ from Ref. 11. ▲ and ▼ are our ground-state results for ΔE_1 and ΔE_2 for $N=20$, respectively.

in the thermal averages.[21] It should be stressed that the FTLM gives also the correct ground state within the chosen small system.

III. THERMODYNAMIC PROPERTIES

Thermodynamic properties $\mathcal{O}(c_h)$ depend on the hole concentration $c_h=N_h/N$. For the weak doping limit, one would expect a linear dependence for most quantities. For a finite system size, the relevant parameter is thus the number of holes, N_h, doped into the AFM. In the low-doping regime, it makes sense to represent the results as a difference

$$\Delta\mathcal{O}_i=\mathcal{O}(N_h=i)-\mathcal{O}(N_h=i-1). \qquad (11)$$

To distinguish the change in a particular quantity with doping, this notation is used in the following. If, e.g., $\Delta\mathcal{O}_2$ behaves quantitatively as $\Delta\mathcal{O}_1$, one can conclude that the quantity changes linearly with the number of added holes, N_h; i.e., the holes behave as independent entities, and the system sizes are large enough so that the low-doping regime has indeed been reached. Such behavior is, however, not the only possibility at low doping, since one can expect, e.g., even-odd effects in the case of pairing of holes.

A. Internal energy, specific heat, and entropy

The internal energy, defined by

$$E=\frac{\partial\beta F}{\partial\beta}=-\frac{1}{Z}\frac{\partial Z}{\partial\beta}, \qquad (12)$$

is calculated within the FTLM as $\langle E\rangle$ in Eq. (10) and in QMC as an expectation value of the corresponding operator, $E=\Sigma_\mathcal{C}E(\mathcal{C})W(\mathcal{C})$. Results of both methods are presented in Fig. 2.

From Fig. 2 we first conclude that for ΔE_1 the results at $N=20$ (which overlap also with the results at $N=18$) obtained via the FTLM are essentially equivalent with QMC results for much larger lattices, at least for $T\gtrsim0.2t$ reached by the QMC method. We note also a close agreement between QMC ΔE_2 and ΔE_1, confirming the assumption of the low-doping regime and holes as independent quasiparticles in the T window presented. In FTLM results, on the other hand, the difference between ΔE_2 and ΔE_1 is already visible, since $N_h=2$ here means already an appreciable doping $c_h=0.1$. For $T=0$ the difference $\Delta E_2-\Delta E_1$ equals to the binding energy[11] and in the continuum corresponds to the second derivative of the ground-state energy with respect to the doping. In the chosen parameter regime ($J=0.4t$), the binding energy is negative, thus pointing to an attractive interaction between the holes. With the increase of the temperature, the bound state disintegrates and the difference $\Delta E_2-\Delta E_1$ approaches zero. In the case of a small system, the difference can even become positive, but vanishes with increasing system size.

It is also evident from Fig. 2 that $\Delta E(T)$ is not a monotonous function. The ground state of a single hole introduced into the AFM is quite well understood via analytical approaches[22] and numerical calculations.[11] For $J/t=0.4$, the zero-temperature result $\Delta E(0)\sim-1.44t$ can be explained well by the interplay between the gain of the kinetic energy represented by the hopping term H_t and the loss of local AFM correlation energy around the hole.

$\Delta E(T)$ has not been considered so far. An interpretation of its behavior can be given as follows. Introducing a single hole into an AFM destroys the local AFM spin order and thus increases the exchange energy. The increase is, however, expected to disappear at $T>J$ where the spin system becomes disordered. On the other hand, the ground-state kinetic energy in a disordered spin system is quite similar to the one in an AFM, hence the decrease of the internal energy ΔE for $T>J$. This remains valid for $T<t$ where also higher hopping-related states become populated and finally $\Delta E(T\to\infty)\to0$, explaining the turn back up for $T\gtrsim0.7t$.

The specific heat defined by

$$C=\frac{\partial E}{\partial T}=\beta^2\left[\frac{1}{Z}\frac{\partial^2Z}{\partial\beta^2}-\left(\frac{1}{Z}\frac{\partial Z}{\partial\beta}\right)^2\right] \qquad (13)$$

is obtained as $\beta^2[\langle E^2\rangle-\langle E\rangle^2]$ within the FTLM and the QMC method. The results are presented in Fig. 3.

The main effect of introducing holes into the AFM insulator on C is to decrease the peak at $T\sim J$. This appears in ΔC as a pronounced dip which slightly weakens and shifts its energy scale J to lower values with doping, as can be seen from the line shape in Fig. 3.

The entropy is

$$S=\beta(E-F)=\beta E+\ln Z. \qquad (14)$$

We reconstruct it from the specific heat

$$C=T\frac{\partial S}{\partial T} \qquad (15)$$

by numerical integration from high temperatures $T\sim\infty$:

$$\Delta S(T)-\Delta S(\infty)=\int_\infty^T\frac{\Delta C}{T}dT. \qquad (16)$$

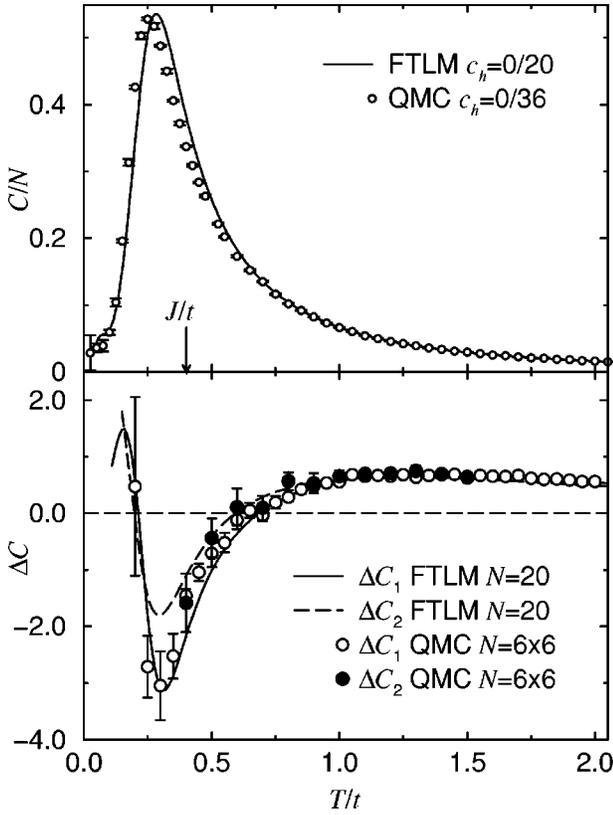The high-temperature integration constants are chosen so that $\Delta S(\infty)=\Delta\ln N_{st}$.

FIG. 3. Specific heat per site C/N for undoped system (top) and change with doping ΔC (bottom, both in units of k_B) vs T as calculated within the FTLM and the QMC method for $J=0.4t$.

In contrast to ΔE and ΔC discussed previously, ΔS is not linear in N_h in the low-doping limit. In analogy with low-concentration systems, like the dilute classical gas, entropy is expected to scale as $\Delta S \propto |\Delta(N_{C_h} \ln_{C_h})|$, i.e., $\Delta S_1 \propto \ln N$, so the change still depends explicitly on the system size. This is also realized in Fig. 4, where ΔS_1 still varies with N, yet curves for different N appear parallel down to the lowest reachable temperatures.

It is particularly remarkable how large the entropy increase $\Delta S_1 \gg 1$ is even at the lowest $T<J$. This is indeed

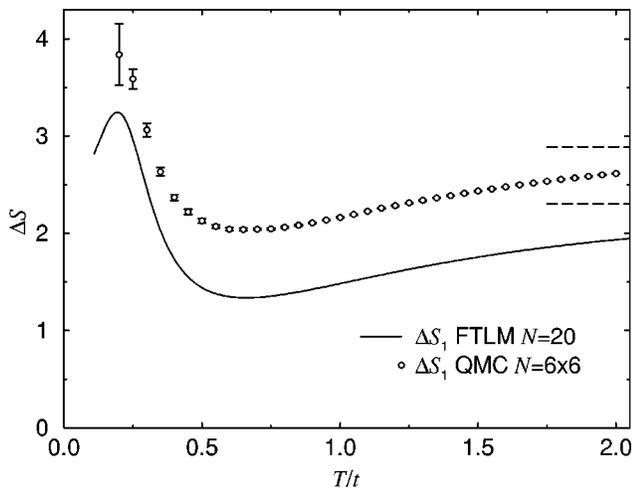FIG. 4. Entropy increase ΔS (in units of k_B) for a single hole obtained via the FTLM and the QMC method, on different size lattices and $J=0.4t$. Long-dashed lines represent $\Delta S(\infty)$.
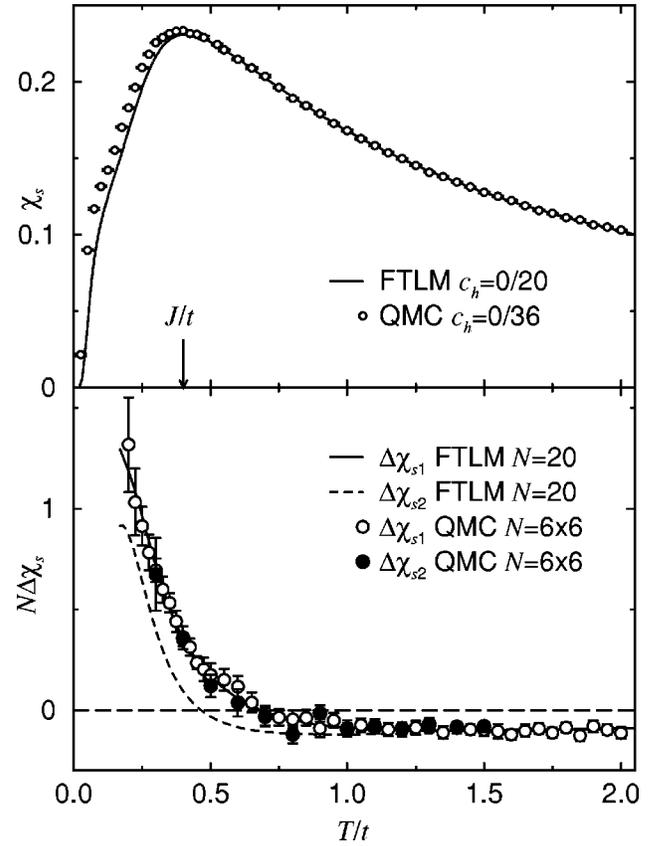

FIG. 5. Spin susceptibility for undoped system χ_s (top) and change of the spin susceptibility with doping $\Delta\chi_s$ (bottom) vs T obtained within the FTLM and the QMC method for $J=0.4t$.

consistent with ΔS measured in cuprates.[23] While this could be attributed partly to the logarithmic dependence on c_h, at the same it is evident that the behavior is much closer to a system of classical particles than to a degenerate electron gas.

B. Spin susceptibility

The uniform spin susceptibility can be evaluated as a thermodynamic quantity from

$$\chi_s = \frac{\beta \langle S_z^2 \rangle}{N}, \qquad (17)$$

where $S_z = \Sigma_i S_i^z$ is the conserved total spin. In the FTLM then Eq. (10) can be applied, while within the QMC method χ_s is related to the number of spin-up and -down WLs.

It is instructive to present results both for $\Delta\chi_s$ with respect to the undoped AFM, Fig. 5, as well as for the effective Curie constant (difference of the square moment) per hole, $\Delta\langle S_z^2 \rangle = N\Delta\chi_s / \beta$, in Fig. 6.

The results in Figs. 5 and 6 are easy to interpret for high $T>t$. Each hole introduced into the system reduces the effective Curie constant by one spin, i.e., $\Delta\langle S_z^2 \rangle = -1/4$. On the other hand, at low $T<J$ the situation is reversed since $\Delta\chi_s > 0$. This increase can be attributed to the relaxation of the AFM order by the hole doping. Note that in an AFM, χ_s achieves a maximum at $T \sim J$, while below that temperature it is reduced due to the longer-range AFM order. It is inter-
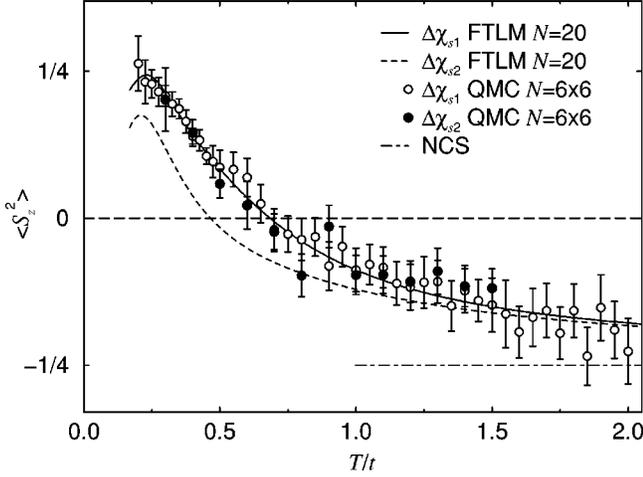
FIG. 6. Effective square moment (Curie constant) per hole $\Delta\langle S_z^2\rangle$ vs T, obtained from the data in Fig. 5. For comparison also the result for noninteracting classical spins (NCSs) is presented (dashed line).

esting to note that at the lowest reachable temperature $T \sim J/2$ each hole effectively adds just one spin, i.e., $\Delta\langle S_z^2\rangle \sim 1/4$.

IV. ORBITAL SUSCEPTIBILITY

In order to investigate the orbital response of the system, a homogeneous magnetic field B perpendicular to the plane has to be introduced. When we discuss the orbital magnetization and susceptibility, B enters only in the kinetic term of Eq. (1), via the Peierls construction

$$H_t = -t \sum_{\langle ij \rangle \sigma} (e^{i\theta_{ij}}\widetilde{c}_{j\sigma}^\dagger \widetilde{c}_{i\sigma} + \text{H.c.}), \quad (18)$$

where the phases are given within Landau gauge as

$$\theta_{ij} = \frac{e}{\hbar}\mathbf{A}(\mathbf{r}_i)\cdot\mathbf{R}_{ij}, \quad \mathbf{A} = B(0,x,0), \quad (19)$$

with $\mathbf{R}_{ij} = \mathbf{r}_j - \mathbf{r}_i$. The relevant parameter for the strength of B is the dimensionless flux per plaquette $\alpha = 2\pi Ba^2/\phi_0$, where a is the lattice spacing and $\phi_0 = h/e$ is the unit quantum flux.

The dc orbital susceptibility of the system in the external magnetic field is

$$\chi_d = -\mu_0 \frac{\partial^2 F}{\partial B^2} = -\frac{\mu_0 e^2 a^4}{\hbar^2}\frac{\partial^2 F}{\partial \alpha^2}$$

$$= -\frac{\chi_0}{\beta}\left[\frac{1}{Z}\frac{\partial^2 Z}{\partial \alpha^2} - \left(\frac{1}{Z}\frac{\partial Z}{\partial \alpha}\right)^2\right], \quad (20)$$

where $\chi_0 = \mu_0 e^2 a^4/\hbar^2$. So far, χ_d has been investigated only for a single hole $N_h = 1$ by a high-temperature expansion at $J = 0$, and by the FTLM for $J > 0$.[9] In the latter study it was realized that results are quite sensitive to finite-size effects, so it is desirable to get corresponding results also via the QMC method, where much larger lattices can be studied.

Let us first derive the expression for the orbital susceptibility within the QMC method. As seen from Eq. (18), the magnetic field affects only the hopping of the electrons. In

the WL representation this concerns matrix elements $\langle\phi|e^{-\tilde\beta H}|\phi'\rangle$ in Eq. (2). For the plaquette representing the hopping between sites i and j, the matrix elements become

$$H_{ij}^{\text{hop}} = \begin{pmatrix} 0 & -te^{i\theta_{ij}} \\ -te^{-i\theta_{ij}} & 0 \end{pmatrix}, \quad (21)$$

written in the $|\circ\uparrow\rangle, |\uparrow\circ\rangle$ base. The imaginary time propagator in the same base is

$$e^{-\tilde\beta H_{ij}^{\text{hop}}} = \begin{pmatrix} \cosh\tilde\beta t & e^{i\theta_{ij}}\sinh\tilde\beta t \\ e^{-i\theta_{ij}}\sinh\beta t & \cosh\tilde\beta t \end{pmatrix}. \quad (22)$$

Thus the plaquette weights along the hole WL obtain an additional phase factor $W(p,\alpha) = W(p)e^{i\theta(p)}$. The weight of the whole configuration is a product, Eq. (3),

$$W(\mathcal{C},\alpha) = \prod_{p\in\mathcal{C}} W(p,\alpha) = W(\mathcal{C})\prod_{p\in\mathcal{C}}\exp[i\theta(p)], \quad (23)$$

where the phases sum up:

$$\exp\left[i\sum_{p\in\mathcal{C}}\theta(p)\right] = \exp\left[i\oint\theta(\mathbf{r})d\mathbf{r}\right]$$

$$= \exp\left[i\frac{e}{\hbar}\oint\mathbf{A}(\mathbf{r})d\mathbf{r}\right] = e^{i\alpha\mathcal{S}}. \quad (24)$$

The integral runs along the hole WL. Here $\mathcal{S}$ is defined as the oriented area of the hole WL projected onto the plane in units of the lattice plaquette area a^2. For more holes, $\mathcal{S}$ generalizes similarly to the sum of all hole WL areas.

Now we can write the partition function in the magnetic field as

$$Z = \sum_{\mathcal{C}} W(\mathcal{C},\alpha) = \sum_{\mathcal{C}} e^{i\alpha\mathcal{S}(\mathcal{C})}W(\mathcal{C}). \quad (25)$$

For a given configuration $\mathcal{C}$, there always exist $\mathcal{C}'$ (imaginary time inversion) with the same weight, but $\mathcal{S}(\mathcal{C}') = -\mathcal{S}(\mathcal{C})$; therefore, the exponential in Eq. (25) can be replaced by a cos function. For $B = 0$ we have $\langle\mathcal{S}\rangle = 0$ and obtain the zero-field susceptibility from Eq. (20),

$$\chi_d = -\chi_0\frac{\langle\mathcal{S}^2\rangle}{\beta}. \quad (26)$$

χ_d can be thus measured without the presence of a magnetic field. This is just another consequence of the more general fluctuation-dissipation theorem. Even though $\mathcal{S}^2$ is strictly positive, the thermal average in Eq. (26) can become negative because of correlations between the sign of the weight and the area $\mathcal{S}$ of the hole WL. From Eq. (6) we can deduce that $\langle\mathcal{S}^2\rangle < 0$ when the configurations with negative sign tend to have larger $\mathcal{S}^2(\mathcal{C})|W(\mathcal{C})|$ than configurations with positive ones.

The hole WL can obtain nonzero spatial winding number due to the periodic boundary conditions and small system size. E.g., the WL can run along the imaginary time, cross the system boundary, and complete time periodicity reconnecting with its spatially periodic image. In that case the area $\mathcal{S}$ as defined by Eq. (24) has no physical meaning. Therefore, we restrict our simulation so that only the zero spatial wind-
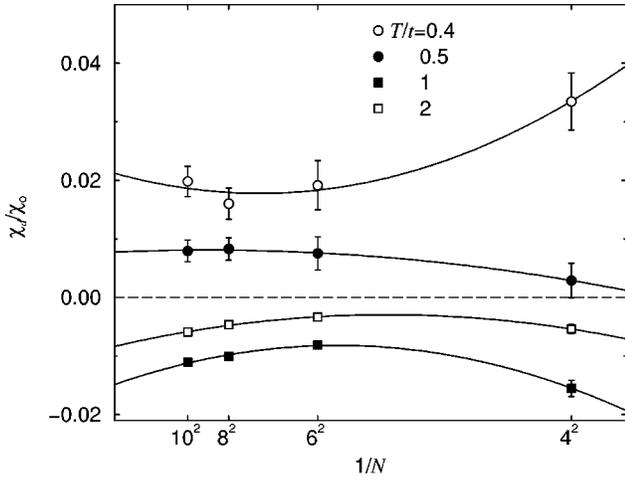
FIG. 7. Finite-size scaling of χ_d from QMC with one hole, for different T and $J = 0.4t$. Solid lines serve as a guide to the eye and are fits to the $1/N^2$ and $1/N^4$ dependence.

FIG. 8. Orbital susceptibility χ_d vs T obtained via the QMC method and the FTLM for $J = 0.4t$. Regarding the FTLM, χ_{12} for $N = 20$ should be most relevant (thick line).

ing loop updates are generated (a discussion on fixing the winding numbers can be found in Ref. 24). The hole is allowed to cross the system boundary as long as it does not increase the winding number. The effect of the restriction is analogous to the movement of the hole doped into an infinite periodic spin background with a unit cell equal to the size of the system. The results for thermodynamic quantities presented in the previous section agree within the error bars with the unrestricted case. This restriction is weaker than closed boundary conditions, resulting in smaller finite-size effects.

The introduction of finite $B > 0$ into the model, Eq. (18), reduces the translational symmetry and thus for a given system size increases the required minimal base set used in the FTLM. In the present study a few mobile holes on a system of tilted squares with N up to 20 sites and periodic boundary conditions are considered. It is nontrivial to incorporate phases θ_{ij} corresponding to a homogeneous B, being at the same time compatible with periodic boundary conditions.[25,9] This is possible only for quantized magnetic fields $B = mB_0$, where $B_0 = \phi_0/N$.

χ_d from Eq. (26) can be calculated in the FTLM only by taking a numerical derivative of the free energy $F = -T \ln Z$, with Z from Eq. (9). Finite systems provide $F(\alpha)$ only for discrete values of α. Here χ_d can be obtained by fitting the $F(\alpha)$ dependence to the parabolic form $F(\alpha) = F(0) + c\alpha^2$ in two points $\alpha = i2\pi/N$ and $\alpha = j2\pi/N$. The corresponding results for the susceptibility are denoted by χ_{ij}. In small systems ($N < 20$) the introduction of $B > 0$ can lift some zero-field degeneracies. The χ_{01} values are therefore systematically affected by larger finite-size effects. For the system with $N = 20$, both values χ_{01} and χ_{12} agree quite reasonably with the QMC data.

Let us first comment on the validity of results for χ_d. Since χ_d deals with an orbital current represented by loop motion of charge carriers (holes), it is much more sensitive to finite-size effects[9] than most other correlation functions. This was also the main motivation to employ the QMC method, where much larger systems can be reached. In Fig. 7, finite-size scaling is performed for the QMC data for $\chi_d(T)$ for the case of $N_h = 1$. We can see that the different T
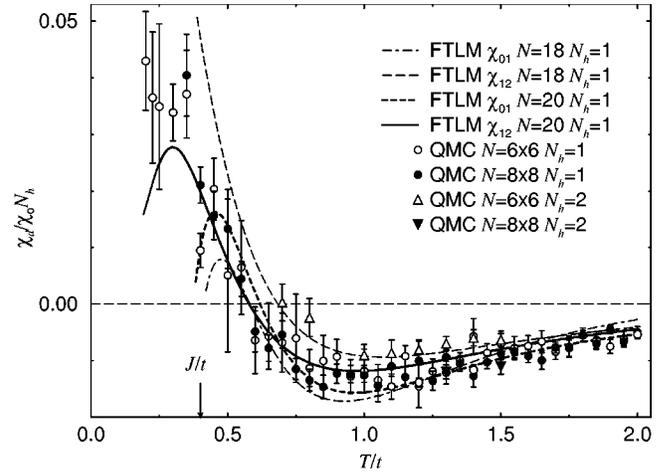
points do not cross upon changing the system size N. Thus, at least qualitatively, results do not depend on the system size. Therefore, the sizes of choice for the QMC systems will be 6×6 and 8×8.

In Fig. 8, χ_d obtained via both methods is presented. For $T \gg t$, the response is diamagnetic and proportional to T^{-3} as well as essentially J independent.[9] The most striking effect is that the orbital response below some temperature T_p turns from diamagnetic to paramagnetic, consistent with the preliminary results obtained via the FTLM.[9] In order to locate the origin of this phenomenon, results for different J and anisotropies γ are shown in Fig. 9. It appears that T_p scales with γJ: i.e., at $J = 0$ the response is clearly diamagnetic at all T, and for $\gamma = 0$, $J > 0$ no crossing is observed with either method.

At lower temperatures $T < T_d \ll T_p$, the diamagnetic behavior is expected to be restored. This follows from the ar-
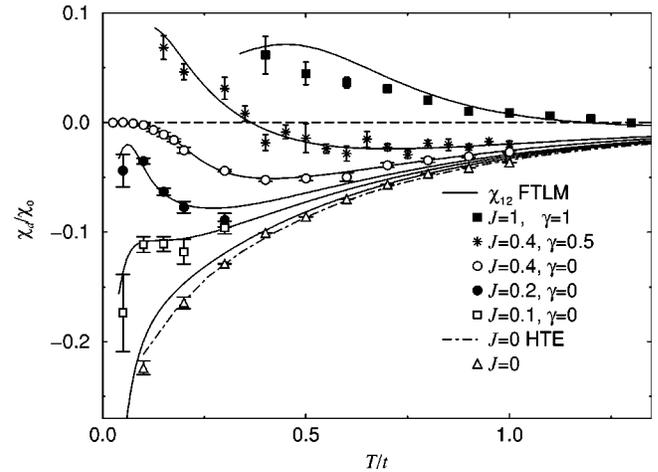

FIG. 9. χ_d vs T for $N_h = 1$ and different J and γ. QMC results for the 6×6 system are shown with different dots and are labeled with appropriate values of J and γ. Solid lines correspond to the $N = 20$ FTLM for the same values of J, γ as in QMC. For comparison also results of a high-temperature expansion (HTE) for $J = 0$ (Ref. 9) are shown (dash-dotted line). The data for $J = 0.4$, $\gamma = 1$ from Fig. 8 are not shown again.
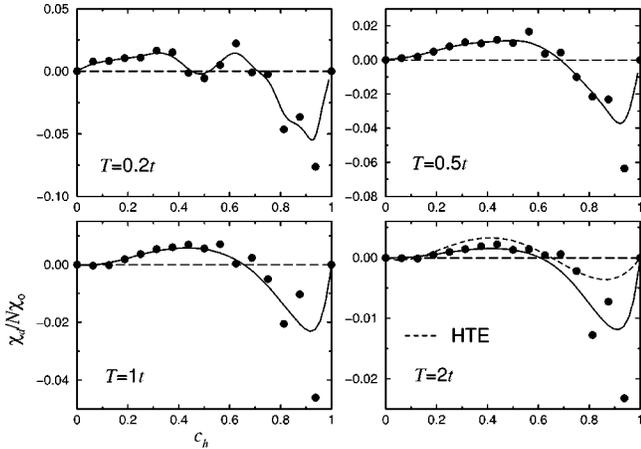
FIG. 10. χ_d vs c_h for several T and $J=0.4t$. The last graph contains also a fourth-order HTE result (dotted line). Canonical (dots) and grand-canonical (line) values for all c_h are obtained within the FTLM with $N=16$, where χ_{12} is used to calculate χ_d.

gument that at $T\rightarrow 0$ a hole in an AFM should behave as a quasiparticle with a finite effective mass, exhibiting a cyclotron motion in $B\neq 0$. The latter behavior should lead to $\chi_d(T\rightarrow 0)\rightarrow -\infty$.[9] Numerically, it is easiest to test this conjecture for a single hole and $\gamma=0$ (also true for $J=0$). Namely, the QMC has no sign problem at $\gamma=0$, so that error bars are only due to the finite MC sampling.

The results in Fig. 9 are quite interesting even for $\gamma=0$. At $J=0$ a monotonous increase of $|\chi_d|$ is observed, diverging as $T\rightarrow 0$.[9] It can be explained as a gradual transition from a hole in a random spin background to a well-defined quasiparticle, i.e., the ferromagnetic polaron, at $T\rightarrow 0$. The situation is more complicated for $J>0$. It is plausible that the difference to the $J=0$ case shows up at $T<J$, where the AFM short-range correlations appear. Relative to $J=0$, a spin-ordered state blocks the loop motion of holes, necessary for finite diamagnetic χ_d. The effect is thus first a decrease of $|\chi_d(T)|$ with decreasing T, as seen in Fig. 9. Turnover to the diverging diamagnetic χ_d should happen only when the coherent quasiparticle is formed at $T_d\ll J$. Here T_d should scale with the inverse of the quasiparticle effective mass $1/m^*$. It is known that m^* can become very large for the extreme $\gamma=0$ case, in particular for larger J. This explains why we cannot reach the coherent regime for $J=0.4t$ even at $T=0.2t$ (Fig. 8), while the downturn is indeed observed for $J/t=0.1$, 0.2, $\gamma=0$ (Fig. 9).

At $\gamma>0$, the results are qualitatively different. The most pronounced effect is the change into a paramagnetic χ_d for $T<T_p$. The width of this T window is quite large. In fact, within the FTLM and QMC data we are unable to locate the reentrance temperature T_d into the diamagnetic response, although the latter is expected.[9] An argument for the low value of T_d can be given in terms of a very shallow energy minimum which defines the quasiparticle dispersion near the ground state of a hole in an AFM within the t-J model,[11] and hence the quasiparticle loses its character already at very low excitation energies. Still, the paramagnetic response in the window $T_d<T<T_p$ remains to be explained.

Let us finally discuss also results for χ_d for finite doping $c_h>0$, as presented in Fig. 10. The easiest regime to interpret is that of a nearly empty band, i.e., $c_h>0.7$, where χ_d is

diamagnetic and nearly independent of T. In this regime the electron system is dilute and strong correlations are unimportant; hence, Landau diamagnetism is expected. At moderate temperatures $T>J$ and for an intermediate-doping regime, $0.2<c_h<0.7$, χ_d is dominated by a paramagnetic response with a peak at approximately $c_h=1/2$. As consistent with results at low doping, there is a weak diamagnetism at $c_h<0.2$ and $T>T_p$, while the paramagnetic regime extends to $c_h=0$ for $T<T_p$. For low temperatures $T\ll J$ quite pronounced oscillations in $\chi_d(c_h)$ appear and can be partly attributed to finite-system effects.

Certain aspects of the above results for $\chi_d(c_h)$ can be understood using the HTE. One is the asymmetry between $c_h\rightarrow 0$ and $c_h\rightarrow 1$ at higher $T>t$. In the lowest order of the HTE, only hopping of the electrons around a basic plaquette loop has to be considered. The signal on the $c_h\rightarrow 0$ side of $\chi_d(c_h)$ is thus reduced by a factor of $2^3=8$ against the $c_h\rightarrow 1$ side since in the first case only the plaquettes with ferromagnetically aligned spins contribute.

V. CONCLUSIONS

Let us first compare both numerical methods used in the analysis of the t-J model at low doping. The QMC method allows the studies of larger systems and the loop algorithm solves some serious drawbacks of the MC methods. It is indeed very efficient in cases where there is no sign problem, e.g., the anisotropic model $\gamma=0$ at $N_h=1$. Within the WL approach it is also very easy to formulate and measure certain responses like the orbital susceptibility χ_d. Still, the method suffers from a sign problem (for $\gamma>0$) even for a single hole $N_h=1$ in an AFM (though not in a background of no holes[14]). Results are thus in practice limited to $T\gtrsim J/3$ for the isotropic case $\gamma=1$. On the other hand, the FTLM has no minus-sign problem, but rather limitations due to small systems which can be studied. These are even more pronounced in cases with $B>0$ where the translational symmetry is lost. It is an interesting observation that within the FTLM, the limiting temperature T_{fs} for the t-J model is in most cases quite close to the lowest T reached by the QMC method.

We have presented several results for thermodynamic quantities, i.e., energy E, specific heat C, entropy S, and spin susceptibility χ_s, as a function of T at low doping. At $T>T_{fs}$ all results are consistent with the picture where holes introduced into the AFM behave as independent (nondegenerate) particles. The perturbation introduced into the AFM by holes is quite large even at lowest $T<J$, in particular visible from ΔC and ΔS, consistent with experiments in cuprates.[23]

Results for the orbital susceptibility χ_d, now obtained also for much larger systems using the QMC method, confirm the preliminary FTLM results,[9] indicating an anomalous paramagnetic response at low doping in an intermediate window of temperatures $T_d<T<T_p\sim J$ (for the isotropic model $\gamma=1$). In fact, within our numerical studies it is hard to reach the lower end of this window, meaning that $T_d<J/3$. Still, the reentrance into a diamagnetic behavior is expected from theoretical arguments on the existence of a well-defined quasiparticle at $T\rightarrow 0$, as well as from more reliable QMC results for the $\gamma=0$ case.[9] The paramagnetic response at

intermediate T can be viewed also as an extension of a more pronounced $\chi_d > 0$ regime observed at finite doping $0.2 < c_h < 0.5$ at all T. The explanation can thus go in the direction proposed by Laughlin,[26,8] that at low doping $c_h \to 0$ we are dealing with quasiparticles (with a diamagnetic response), being a bound composite of charge (holon) and spin (spinon) elementary excitations. The binding appears, however, to be quite weak and thus easily destroyed by finite T or c_h, enabling the independent response of constituents, which apparently is paramagnetic.

*Electronic address: darko.veberic@ijs.si

†Electronic address: peter.prelovsek@ijs.si

‡Electronic address: evertz@itp.tu-graz.ac.at

[1] For a review, see M. Imada, A. Fujimori, and Y. Tokura, Rev. Mod. Phys. **70**, 1039 (1998).

[2] B. Batlogg, H. Y. Hwang, H. Takagi, R. J. Cava, H. L. Kao, and J. Kwo, Physica C **235-240**, 130 (1994).

[3] V. J. Emery and S. A. Kivelson, Physica C **209**, 597 (1993).

[4] A. Sokol and D. Pines, Phys. Rev. Lett. **71**, 2813 (1993).

[5] For a review see, e.g., N. P. Ong, in *Physical Properties of High Temperature Superconductors*, edited by D. M. Ginsberg (World Scientific, Singapore, 1990), Vol. 2.

[6] L. Landau, Z. Phys. **64**, 629 (1930).

[7] A. G. Rojo, G. Kotliar, and G. S. Canright, Phys. Rev. B **47**, 9140 (1993).

[8] P. Béran, Phys. Rev. B **54**, 1391 (1996); P. Béran, D. Poilblanc, and R. B. Laughlin, Nucl. Phys. B **473**, 707 (1996).

[9] D. Veberič, P. Prelovšek, and I. Sega, Phys. Rev. B **57**, 6413 (1998).

[10] R. E. Walstedt, R. F. Bell, L. F. Schneemeyer, J. V. Waszczak, and G. P. Espinosa, Phys. Rev. B **45**, 8074 (1992); M. Miljak, V. Zlatić, I. Kos, J. D. Thompson, P. C. Canfield, and Z. Fisk, Solid State Commun. **85**, 519 (1993).

[11] For a review, see E. Dagotto, Rev. Mod. Phys. **66**, 763 (1994).

[12] S. R. White and D. J. Scalapino, Phys. Rev. B **61**, 6320 (2000), and references therein.

[13] H. G. Evertz, G. Lana, and M. Marcu, Phys. Rev. Lett. **70**, 875 (1993); for a review, see H. G. Evertz, in *Numerical Methods for Lattice Quantum Many-Body Problems*, edited by D. J. Scalapino, Frontiers in Physics (Perseus Books, CO, in press).

[14] M. Brunner, F. F. Assaad, and A. Muramatsu, cond-mat/9904150 (unpublished).

[15] B. Ammon, H. G. Evertz, N. Kawashima, M. Troyer, and B. Frischmuth, Phys. Rev. B **58**, 4304 (1998).

[16] M. Brunner and A. Muramatsu, Phys. Rev. B **58**, R10 100 (1998).

[17] H. F. Trotter, Proc. Am. Math. Soc. **10**, 545 (1959); M. Suzuki, Prog. Theor. Phys. **56**, 1454 (1976).

[18] *Quantum Monte Carlo Methods in Condensed Matter Physics*, edited by M. Suzuki (World Scientific, Singapore, 1994), p. 65.

[19] B. B. Beard and U.-J. Wiese, Phys. Rev. Lett. **77**, 5130 (1996).

[20] J. Jaklič and P. Prelovšek, Phys. Rev. B **49**, 5065 (1994).

[21] For a review, see J. Jaklič and P. Prelovšek, Adv. Phys. **49**, 1 (2000).

[22] S. Schmitt-Rink, C. M. Varma, and A. E. Ruckenstein, Phys. Rev. Lett. **60**, 2793 (1988).

[23] J. W. Loram, K. A. Mirza, J. R. Cooper, and W. Y. Liang, Phys. Rev. Lett. **71**, 1740 (1993).

[24] P. Henelius, S. M. Girvin, and A. W. Sandvik, Phys. Rev. B **57**, 13 382 (1998).

[25] E. Fradkin, *Field Theories of Condensed Matter System*, Frontiers in Physics, Vol. 82 (Addison-Wesley, Redwood City, CA, 1991), p. 252.

[26] R. B. Laughlin, J. Low Temp. Phys. **99**, 443 (1995).